Computational high-throughput screening of electrocatalytic materials for hydrogen evolution

JEFF GREELEY[1], THOMAS F. JARAMILLO[2], JACOB BONDE[2], IB CHORKENDORFF[2] AND JENS K. NØRSKOV[1]*

[1]Center for Atomic-scale Materials Design, NanoDTU, Department of Physics, Technical Univ. of Denmark, DK-2800 Kongens Lyngby, Denmark
[2]Center for Individual Nanoparticle Functionality, NanoDTU, Department of Physics, Technical Univ. of Denmark, DK-2800 Kongens Lyngby, Denmark
*e-mail: norskov@fysik.dtu.dk

Published online: 15 October 2006; doi:10.1038/nmat1752

The pace of materials discovery for heterogeneous catalysts and electrocatalysts could, in principle, be accelerated by the development of efficient computational screening methods. This would require an integrated approach, where the catalytic activity and stability of new materials are evaluated and where predictions are benchmarked by careful synthesis and experimental tests. In this contribution, we present a density functional theory-based, high-throughput screening scheme that successfully uses these strategies to identify a new electrocatalyst for the hydrogen evolution reaction (HER). The activity of over 700 binary surface alloys is evaluated theoretically; the stability of each alloy in electrochemical environments is also estimated. BiPt is found to have a predicted activity comparable to, or even better than, pure Pt, the archetypical HER catalyst. This alloy is synthesized and tested experimentally and shows improved HER performance compared with pure Pt, in agreement with the computational screening results.

The *in silico* design of functional materials on the basis of electronic-structure calculations is a longstanding goal of theoretical materials science. Such an effort would require the establishment of a direct link between the macroscopic functionality and the atomic-scale properties of the material, in addition to the development of efficient and accurate methods for solving the electronic-structure problem. The first examples of the use of computational methods to screen for new materials have recently been published[1–10]. Such calculations are computationally demanding, and these studies have generally either used simplified electronic-structure schemes or have considered relatively few material combinations. In the present article, we show that it is possible to carry out moderately large-scale combinatorial screening for alloy catalyst materials using density functional theory (DFT) calculations. We introduce a screening procedure that efficiently combines catalytic activity criteria, detailed stability assessments and a database of DFT calculations on more than 700 binary transition-metal surface alloys. We apply the procedure to the evaluation of alloy catalysts for a fundamental electrochemical process, the hydrogen evolution reaction (HER). One of the most promising candidate materials resulting from the search is a surface alloy of bismuth and platinum. We develop a method to synthesize a BiPt surface alloy and show experimentally that its activity is superior to that of Pt, the archetypical HER catalyst.

The HER, which involves proton reduction and concomitant hydrogen evolution, is important for a variety of electrochemical processes, and technological interest in the HER is spread over applications as diverse as hydrogen fuel cells, electrodeposition and corrosion of metals in acids and storage of energy via H_2 production[11–13]. We choose the HER to illustrate our approach primarily because a simple atomic-scale descriptor for the catalytic activity has previously been established. It has long been known that when the catalytic activity of a material for the HER is plotted as a function of the hydrogen–metal bond strength, a volcano-shaped form is found[14–18]. This behaviour is related to the Sabatier

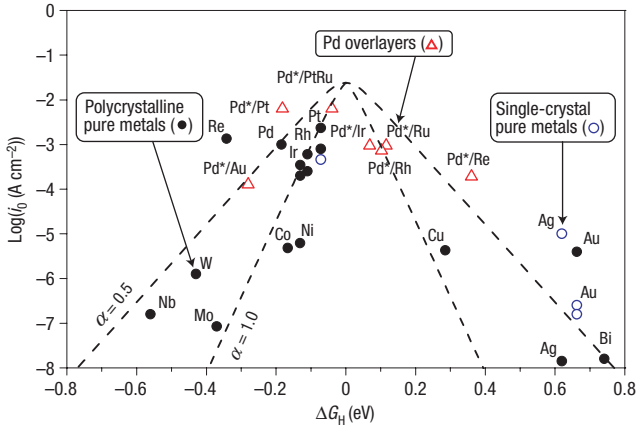

Figure 1 Volcano plot for the HER for various pure metals and metal overlayers. ΔG_H values are calculated at 1 bar of H_2 (298 K) and at a surface hydrogen coverage of either 1/4 or 1/3 ML. Experimental data are compiled in refs 17,20,21. Where available, computational data are taken from the present work; other computational results are taken from the references above. The experimental data have been collected from over 40 years of publications, representing different experimental conditions and surface structures. No corrections for changes in the calculated ΔG_H values with coverage are included, in contrast to the calculated values for Pd overlayers (denoted by Pd*/substrate) presented in ref. 21. The two curved lines correspond to the activity predictions of simple mean-field, microkinetic models, assuming transfer coefficients (α) of 0.5 and 1.0, respectively.

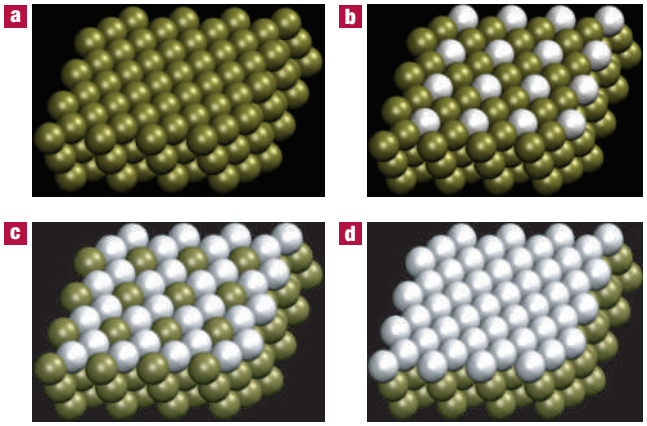

Figure 2 Schematic diagrams of surface alloys at the solute coverages for which calculations are carried out. The solute atoms are shown in white, and the host (substrate) atoms are indicated in dark green. All solute atoms are embedded in the surface layer of the corresponding host metal. **a**, A pure metal. **b**, A surface alloy with solute coverage = 1/3 ML. **c**, A surface alloy with solute coverage = 2/3 ML. **d**, One ML of solute atoms, forming an overlayer.

principle, a general explanatory paradigm in heterogeneous catalysis and electrocatalysis that states that optimal catalytic activity can be achieved on a catalytic surface with intermediate binding energies (or free energies of adsorption) for reactive intermediates[19]. If the intermediates bind too weakly, it is difficult for the surface to activate them, but if they bind too strongly, they will occupy all available surface sites and poison the reaction; intermediate binding energies permit a compromise between these extremes. In the particular case of hydrogen evolution, it turns out that these general principles can be quantified by analysing the free energy of hydrogen adsorption ΔG_H; this quantity is a reasonable descriptor of hydrogen evolution activity for a wide variety of metals and alloys[15,20,21]. As first suggested by Parsons[15], the optimum value should be around $\Delta G_H = 0$. In Fig. 1, we have plotted experimentally measured HER exchange current densities[17,20,21] against ΔG_H values calculated using DFT (see below). Although there is some scatter in the data (the experimental values are from several different authors), the figure seems to suggest that an optimum in the measured HER exchange current densities is found for DFT-derived ΔG_H values very close to (if not identically equal to) zero. We have therefore adopted the approach of using calculated values of $|\Delta G_H|$ to search for new HER catalysts, and we will assume in the following that the closer $|\Delta G_H|$ is to zero, the better the catalyst.

Using periodic ($(\sqrt{3} \times \sqrt{3})R30°$ unit cell), self-consistent, DFT calculations (see the Methods section), we evaluate the value of ΔG_H on the 736 distinct binary transition-metal surface alloys that can be formed from the 16 metals Fe, Co, Ni, Cu, As, Ru, Rh, Pd, Ag, Cd, Sb, Re, Ir, Pt, Au and Bi (these elements are simply chosen to give a very broad pool of metallic and semimetallic elements, most of which are thermodynamically resistant to bulk oxide formation in water at 298 K and $U = 0$ V versus the standard hydrogen electrode; SHE). Such alloys, which are composed of a pure metal substrate with a solute element alloyed into the surface layer (Fig. 2), can exhibit surface properties that are vastly different from the properties of the bulk alloy. In Fig. 3, we show schematically the calculated free energies of hydrogen adsorption on a subset of these surface alloys—those with a 1/3 monolayer (ML) of solute in the surface layer (also see Fig. 2b). The figure clearly demonstrates that a number of binary surface alloys have high predicted activity for the HER.

Our purely computational screening procedure thus identifies a number of interesting candidates for HER catalysts. However, the analysis has so far neglected any consideration of whether or not the indicated alloys will be stable in real electrochemical environments. To estimate the stability of the surface alloys for the HER, we carry out four simple tests for each alloy (see the Supplementary Information). First, we estimate the free-energy change associated with surface segregation events; such events can cause surface solute atoms to segregate into the bulk. Second, we determine the free-energy change associated with intrasurface transformations such as island formation and surface de-alloying. Third, we evaluate the free energy of oxygen adsorption, beginning with splitting of liquid water; facile oxygen adsorption can lead to surface poisoning and/or oxide formation. Finally, we estimate the likelihood that the surface alloys of interest will corrode in acidic environments (pH = 0). For this test, we simply take the free energies of dissolution as reported in the electrochemical series[13].

In Fig. 4, we plot the most pessimistic of the free-energy transformation values determined for each alloy against the absolute magnitude of ΔG_H. The stability considerations immediately eliminate a large number of alloys from consideration; although many alloys have high predicted HER activity, only a small fraction are predicted to be both active and stable in acidic HER environments (Fig. 4), including, among others, surface alloys of BiPt, PtRu, AsPt, SbPt, BiRh, RhRe, PtRe, AsRu, IrRu, RhRu, IrRe and PtRh (note that the last seven of these have solute coverages different from 1/3 ML and therefore are not found in Fig. 3). Thus, these results demonstrate that stability considerations are essential for finding realistic candidate catalysts for hydrogen evolution. Furthermore, the results suggest that more detailed computational analyses and, ultimately, experimental testing of the promising alloys are in order.

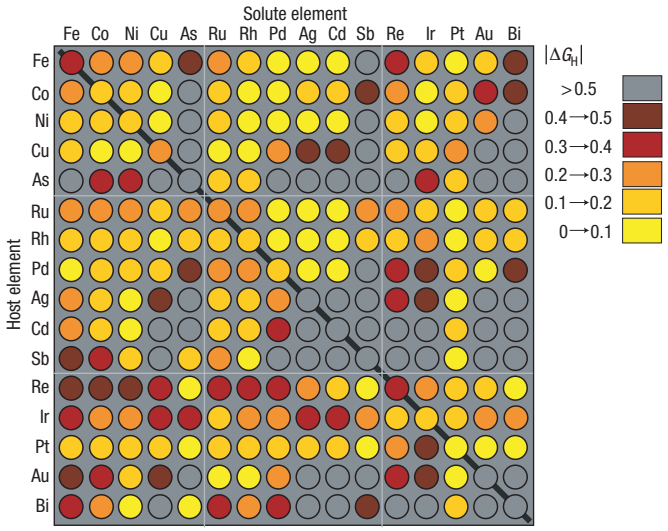

Figure 3 Computational high-throughput screening for $|\Delta G_H|$ on 256 pure metals and surface alloys. The rows indicate the identity of the pure metal substrates, and the columns indicate the identity of the solute embedded in the surface layer of the substrate. Thus, a point at the intersection of the 'Rh' row with the 'Pd' column, for example, would correspond to a surface alloy with Pd embedded in the (111) surface layer of a pure Rh host. The solute coverage is 1/3 ML in all cases, and the adsorbed hydrogen coverage is also 1/3 ML. The diagonal of the plot corresponds to the hydrogen-adsorption free-energy on the pure metals.

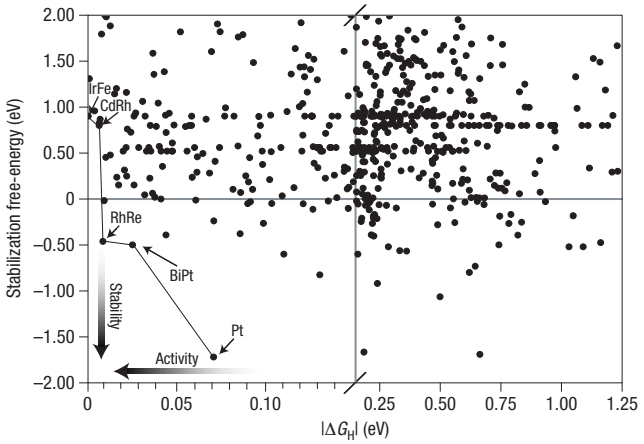

Figure 4 Pareto-optimal plot of stability and activity of surface alloys for the HER. The stabilization free-energy can be thought of as a free energy of formation for the surface alloys; the stability of the alloys with respect to various reconstructive/deactivating processes (including surface segregation, island formation, water splitting/oxygen adsorption and metal dissolution) is evaluated for each alloy, and the most pessimistic such energy (that is, the energy that would give the maximum probability that the alloy would destabilize) is plotted. The Pareto-optimal line indicates the best possible compromise between activity and stability, but given the simplicity of our model, other alloys could certainly be worth considering for use as HER catalysts; the alloys in the lower left quadrant, in particular, are promising. For the labelled points, a single element indicates a pure metal. For the bimetallic alloys, the solute is listed first; the solute coverages are 1/3 ML (BiPt), 1 ML (RhRe), 1/3 ML (CdRh) and 2/3 ML (IrFe).

For the present study, we have selected BiPt for further analysis. This surface alloy is particularly interesting for the HER because of the stark contrast between its two constituent elements; pure Pt exhibits high catalytic activity, whereas pure Bi is not active at all (see Fig. 1). A surface alloy formed from these two elements, however, yields a material predicted by the calculations to have an activity comparable to, or even better than, pure Pt. We note, in passing, that this 'counterintuitive' surface alloy might not have been investigated without the aid of a combinatorial screening approach to guide the search for new catalysts.

To study this material in more detail, we first carried out further calculations on more detailed structural models to assess the effect of Bi coverage on our results. These calculations were done at a Bi coverage of 1/4 ML (2 × 2 unit cells—see the Methods section); we note that Bi coverages equal to or greater than 1/2 ML caused very large distortions of the alloy surface and, thus, were not considered in detail. The coverage of adsorbed hydrogen was also 1/4 ML in these analyses. Although the preferred site preference for H on the BiPt surface alloy was different for the 2 × 2 versus $(\sqrt{3} \times \sqrt{3})R30°$ unit cells (face-centred cubic and near-top sites, respectively), the trends in ΔG_H values for the BiPt versus Pt slabs (−0.03 versus −0.07 eV on the $(\sqrt{3} \times \sqrt{3})R30°$ slab and 0.00 versus −0.04 eV on the 2 × 2 slab, respectively) were unchanged. For this more detailed analysis, we also carried out additional stability tests. We estimated the potential versus SHE at which hydroxyl will adsorb on the surface after water splitting; a value of ∼0.4 V was obtained by following the procedure described previously[22]. Thus, although hydroxyl (which preferentially adsorbs on a Bi top site) adsorbs at a potential several tenths of a volt lower than atomic oxygen, even this more reactive species will not be present under typical HER conditions. We also evaluated the adatom formation energy for a BiPt surface alloy in the presence of 1/4 ML of adsorbed hydrogen. Adatom formation was found to be endothermic (∼0.07 eV) in the presence of adsorbed hydrogen, suggesting that under typical HER conditions, the stable form is that of the surface alloy, and there will only be a relatively small concentration of Bi adatoms present at equilibrium. These results, when combined with the activity and stability calculations described above, paint a picture of BiPt surface alloys as structurally stable systems that exhibit moderately improved hydrogen evolution kinetics compared with pure Pt. It is important to emphasize, however, that the HER model used is quite simple and that the calculated difference in ΔG_H for BiPt and Pt (∼0.04 eV) is small, given the typical accuracy associated with DFT calculations. Thus, it is only possible to conclude from the computational results that BiPt surface alloys might be interesting for the HER. To validate the results of our computational screening, careful experimental tests are clearly necessary.

Mixed Pt and Bi catalysts have been studied experimentally for decades. The two most commonly reported forms are: (1) a Pt surface modified by irreversibly adsorbed Bi (Pt–Bi_{ir}) and (2) bulk intermetallic PtBi or $PtBi_2$. Interest in bulk intermetallics has recently increased; they are typically investigated for electro-oxidation reactions (see, for example, ref. 23). Literature on the Pt–Bi_{ir} system—the most commonly studied form of mixed Pt and Bi—extends back to the 1970s; many studies focus on the oxidation of H_2, CO and formic acid, in addition to the reduction of O_2 (refs 24–33). Perhaps the most pertinent Pt–Bi_{ir} work is that of Gómez *et al.* who investigated the impact of Bi_{ir} on hydrogen evolution for Pt(100) and Pt(111). They showed that Bi_{ir} severely poisons both Pt surfaces for HER, as evidenced by a significant decrease in current as a function of Bi_{ir} coverage[26,27]. This result seems, at first glance, to contradict our theoretical prediction that mixed Pt and Bi alloys show improved activity for the HER. However, it should be recalled that our calculated BiPt

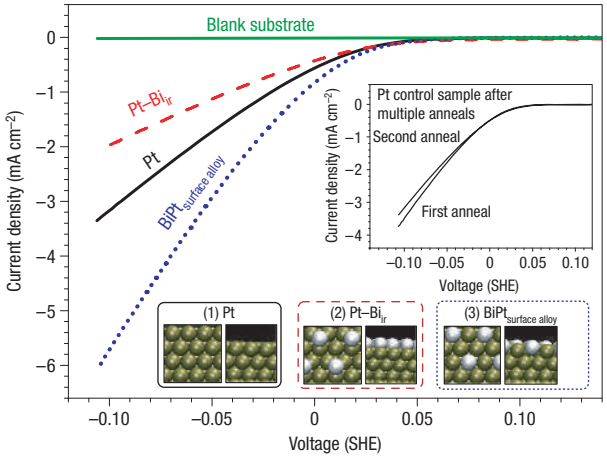

Figure 5 Hydrogen evolution after each stage of BiPt surface alloy synthesis on a fluorine-doped tin-oxide substrate. (1) Pt film after deposition and anneal (2) immediately after Bi UPD (3) after second anneal to form the BiPt surface alloy. The inset represents a control sample—Pt film without Bi—after first and second anneals. Current densities are normalized to the surface area of the initial, pure Pt sample, determined by H UPD.

surface structure is a surface alloy and not Bi_{ir} on Pt. By carefully controlling our electrochemical synthesis procedure (see discussion below), we create a surface alloy, and we show that this specific structure does, in fact, show improved activity for the HER. We note that, to our knowledge, no previous electrochemical studies on the Pt–Bi_{ir} system have attempted to form a surface alloy from the Bi_{ir} submonolayer.

To create the BiPt surface alloy, we used a three-step approach: (1) electrodeposition of an initial Pt film onto an inert support, (2) spontaneous deposition of a submonolayer of Bi_{ir} by Bi underpotential deposition (UPD) and (3) annealing of the Pt–Bi_{ir} precursor to form a BiPt surface alloy. For a given sample, we measured hydrogen evolution after each step of the synthesis. Following the work of Gómez *et al.*, we used the cathodic current density at 0.0 V versus SHE ($i_{0.0\,V}$) as the primary figure of merit for comparison—approximately the exchange current density[26,27,34]. Current–voltage measurements of a representative sample are plotted in Fig. 5. After heating the initial polycrystalline Pt film in a furnace (see the Methods section), the sample demonstrated a current density of $i_{0.0\,V} = 5.6(10)^{-4}\,A\,cm_{Pt}^{-2}$ ($-\log i_{0.0\,V} = 3.25$), consistent with previous literature values for Pt and indicating that the starting material was prepared adequately with negligible contamination[20]. We then adsorbed a submonolayer of Bi_{ir} onto the Pt film by the same Bi UPD method used in previous reports (10 min, 1 mM Bi_2O_3/0.5 M H_2SO_4), resulting in an estimated Bi_{ir} coverage of ~10% by X-ray photoelectron spectroscopy (data not shown). Immediately after Bi UPD, the measured activity of the Pt–Bi_{ir} sample was considerably less than that of the initial Pt film—as expected, the Bi_{ir} blocked Pt sites and poisoned the surface for hydrogen evolution[24]. To complete the synthesis of a BiPt surface alloy, we annealed the Pt–Bi_{ir} precursor to 500 °C in a tube furnace.

Heating the Pt–Bi_{ir} system is the crucial step, as it provides the temperature necessary for Bi to overcome the kinetic barriers associated with alloying into the surface layer of Pt. Evidence of this process was reported by Paffett, Campbell and Taylor who conducted extensive studies of Bi dosed onto a Pt(111) crystal under ultrahigh vacuum conditions[35,36]. They used low-energy electron diffraction and Auger electron spectroscopy to track morphological changes in a Bi adlayer as a function of coverage and temperature. One of the features they observed was that of a multilayered surface alloy—nominal composition $Pt_{1.00}Bi_{0.95}$—that formed at moderate temperatures (~370 °C) after starting with a multilayer Bi film. These surface-science experiments clearly indicate that Bi can and will form a surface alloy with Pt at elevated temperatures. The synthesis procedure that we have developed shows that surface alloys can also be produced from electrochemically adsorbed species; this is a simple, low-cost and general method that can be applied to numerous electrochemical systems.

Having completed the annealing procedure, we again measured the hydrogen evolution rate. Figure 5 shows significantly improved current–voltage characteristics; quantitatively speaking, $i_{0.0\,V}$ is double that of the Pt–Bi_{ir} precursor and, more importantly, ~50% greater than $i_{0.0\,V}$ of the initial Pt film. The improved performance of this film cannot be attributed to a simple change in morphology or to increased surface area because cyclic voltammetry in the H UPD region after each stage of synthesis indicates, if anything, a decrease in Pt surface area (see the Supplementary Information). To verify that the final anneal did not influence the Pt itself, we conducted several control experiments on similarly prepared pure Pt samples through multiple heat treatments. These data are shown as an inset in Fig. 5 and demonstrate a negligible effect.

The three-step procedure used to synthesize the annealed sample is highly reproducible, and the results provide strong evidence that the final, annealed sample is indeed a BiPt surface alloy, consistent with the ultrahigh vacuum studies of Paffett *et al.*[35,36]. It is worth noting that Bi itself is a notoriously poor electrocatalyst for the HER[17]; so it is difficult to imagine a morphology involving Bi—other than a surface alloy—that could possibly improve the electrocatalytic activity of Pt for hydrogen evolution. Hence, we have shown that a combination of *in silico* screening and careful experimental synthesis of promising candidates can lead to improved electrocatalysts, even when the identified metal combinations involve an element that is known to be inert for the HER, or when the metal combinations have previously been studied in different structural forms and have been found to be inactive.

We have thus confirmed experimentally the prediction that the HER activity of BiPt surface alloys should be comparable to that of pure Pt, or perhaps slightly better. This result suggests that our computational screening procedure is a promising technique for use in catalyst searches. The screening procedure can be viewed as a general, systematic, DFT-based method of incorporating both activity and stability criteria into the search for new metal alloy catalysts. As the accuracy and quality of kinetic models and DFT calculations improve, such *in silico* combinatorial screening procedures should become broadly useful for catalytic materials discovery.

METHODS

The computational analysis is carried out using DACAPO[37], a total energy calculation code. For the high-throughput computational screening, a three-layer slab, periodically repeated in a super-cell geometry with five equivalent layers of vacuum between any two successive metal slabs, is used to determine hydrogen binding energies. Close-packed surfaces are considered in all cases. A $(\sqrt{3}\times\sqrt{3})R30°$ unit cell, corresponding to a hydrogen coverage of 1/3 ML, is used. With this unit cell, and using the 16 elements described in the text, it is possible to create 736 symmetrically distinct pure metal and binary surface alloy slabs—16 pure metals, 240 surface alloys with a pure overlayer of solute metal, 240 with only two solute atoms in the surface layer and an extra 240 with one solute atom in the surface layer. For all slabs, the metal atoms are kept fixed in their bulk-truncated positions, and the hydrogen atoms are

allowed to relax until the total force is less than 0.5 eV Å^{-1}. The total energy is then further refined by using the residual forces and estimated harmonic vibrational frequencies for hydrogen (~1,050 cm^{-1} for three-fold sites and ~2,020 cm^{-1} for top sites) to extrapolate to the bottom of a parabola in energy space. 0.24 eV is added to the calculated binding energies (with respect to gaseous H_2) to give adsorption free energies[20]. The oxygen binding energies (used for the oxygen adsorption stability criterion) are computed in the same way, except that a slightly higher force cutoff (0.6 eV Å^{-1}) is used and appropriate vibrational frequencies (~500 cm^{-1} for three-fold sites and ~775 cm^{-1} for top sites) are used for the energy extrapolations.

For all DFT calculations, adsorption is allowed on only one of the two exposed surfaces of the metal slabs, and the electrostatic potential is adjusted accordingly[38]. Ionic cores are described by ultrasoft pseudopotentials[39], and the Kohn–Sham one-electron valence states are expanded in a basis of plane waves with kinetic energy below 340 eV; a density cutoff of 500 eV is used. The surface Brillouin zone is sampled with an $18(\sqrt{3}\times\sqrt{3})$ Chadi–Cohen **k** point grid. In all cases, convergence of the total energy with respect to the cutoff energies and the **k** point set is confirmed. The exchange–correlation energy and potential are described by the generalized gradient approximation[37] (GGA-RPBE98). The self-consistent RPBE98 density is determined by iterative diagonalization of the Kohn–Sham hamiltonian, Fermi population of the Kohn–Sham states ($k_B T = 0.1$ eV) and Pulay mixing of the resulting electronic density[40]. All total energies have been extrapolated to $k_B T = 0$ eV. Zero-point energy effects are assumed to be approximately constant for all metals and alloys considered[20]. Spin-polarization effects are included in the reported results for alloys in which naturally magnetized metals (Ni, Co, Fe) are present. Graphical inserts are produced using visual molecular dynamics[41].

For the more detailed calculations on the BiPt surface alloy, a 2×2 surface unit cell is used, corresponding to a hydrogen coverage of 1/4 ML. A four-layer slab is used for these calculations, and the top two layers of the slab are allowed to relax. The maximum force permitted for any vector component is 0.05 eV Å^{-1}. The **k** point grid, in this case, involves $18(1\times1)$ Chadi–Cohen points.

Pt was electrodeposited from a 1 mM H_2PtCl_6 (99.995%, Aldrich) solution onto an inert substrate—fluorine-doped tin-oxide coated onto glass (Hartford Glass). A square wave pulsed deposition was used, referenced to a Ag quasi-reference electrode (AgQRE). The three-step deposition sequence consisted of a 0.5 s pulse at −0.9 V versus AgQRE, followed by a 0.5 s pulse at −0.2 V versus AgQRE, followed by a 1 s rest interval. The sequence was repeated 120 times, totalling 4 min. The AgQRE was produced by oxidizing a pre-cleaned Ag wire in 1.0 M HCl at +1.0 V versus the saturated calomel electrode for 60 s. Cyclic voltammograms of the deposited and annealed Pt films showed no evidence of contamination, corroborated by X-ray photoelectron spectroscopy measurements. Hydrogen evolution experiments were conducted in N_2-purged H_2SO_4 (pH 0.40). The cyclic voltammogram sweep rate was 5 mV s^{-1} versus the saturated calomel electrode. A bridge was used during recording of the cyclic voltammograms to prevent Cl^- contamination. All heat treatments were conducted in a tube furnace at 500 °C in air for 12 h. Samples were transferred in ambient air and protected in plastic containers.

Received 30 June 2006; accepted 5 September 2006; published 15 October 2006.

References

1. Greeley, J. & Mavrikakis, M. Alloy catalysts designed from first principles. *Nature Mater.* **3,** 810–815 (2004).
2. Muller, R. P., Philipp, D. M. & Goddard, W. A. Quantum mechanical-rapid prototyping applied to methane activation. *Top. Catalys.* **23,** 81–98 (2003).
3. Andersson, M. P. *et al.* Towards computational screening in heterogeneous catalysis: Pareto-optimal methanation catalysts. *J. Catalys.* **239,** 501–506 (2006).
4. Greeley, J., Nørskov, J. K. & Mavrikakis, M. Electronic structure and catalysis on metal surfaces. *Annu. Rev. Phys. Chem.* **53,** 319–348 (2002).
5. Toulhoat, H. & Raybaud, P. Kinetic interpretation of catalytic activity patterns based on theoretical chemical descriptors. *J. Catalys.* **216,** 63–72 (2003).
6. Linic, S., Jankowiak, J. & Barteau, M. A. Selectivity driven design of bimetallic ethylene epoxidation catalysts from first principles. *J. Catalys.* **224,** 489–493 (2004).
7. Ceder, G. *et al.* Identification of cathode materials for lithium batteries guided by first-principles calculations. *Nature* **392,** 694–696 (1998).
8. Besenbacher, F. *et al.* Design of a surface alloy catalyst for steam reforming. *Science* **279,** 1913–1915 (1998).
9. Franceschetti, A. & Zunger, A. The inverse hand-structure problem of finding an atomic configuration with given electronic properties. *Nature* **402,** 60–63 (1999).
10. Vitos, L., Korzhavyi, P. A. & Johansson, B. Stainless steel optimization from quantum mechanical calculations. *Nature Mater.* **2,** 25–28 (2003).
11. Jacobson, M. Z., Colella, W. G. & Golden, D. M. Cleaning the air and improving health with hydrogen fuel-cell vehicles. *Science* **308,** 1901–1905 (2005).
12. Hamann, C. H., Hamnett, A. & Vielstich, W. *Electrochemistry* (Wiley-VCH, Weinheim, 1998).
13. Lide, D. R. (ed.) *CRC Handbook of Chemistry and Physics* (CRC Press, New York, 1996).
14. Conway, B. E. & Bockris, J. O. M. Electrolytic hydrogen evolution kinetics and its relation to the electronic and adsorptive properties of the metal. *J. Chem. Phys.* **26,** 532–541 (1957).
15. Parsons, R. The rate of electrolytic hydrogen evolution and the heat of adsorption of hydrogen. *Trans. Faraday Soc.* **54,** 1053–1063 (1958).
16. Gerischer, H. Mechanism of electrolytic discharge of hydrogen and adsorption energy of atomic hydrogen. *Bull. Soc. Chim. Belg.* **67,** 506 (1958).
17. Trasatti, S. Work function, electronegativity, and electrochemical behaviour of metals. III. Electrolytic hydrogen evolution in acid solutions. *Electroanal. Chem. Interfacial Electrochem.* **39,** 163–184 (1972).
18. Krishtalik, L. I. On the influence of hydrogenation of the cathode metal upon the overvoltage of hydrogen. *Electrokhimiya* **2,** 616 (1966).
19. Sabatier, P. Hydrogénations et deshydrogénations par catalyse. *Ber. Deutschen Chem. Gesellschaft* **44,** 1984 (1911).
20. Nørskov, J. K. *et al.* Trends in the exchange current for hydrogen evolution. *J. Electrochem. Soc.* **152,** J23–J26 (2005).
21. Greeley, J., Kibler, L., El-Aziz, A. M., Kolb, D. M. & Nørskov, J. K. Hydrogen evolution over bimetallic systems: Understanding the trends. *ChemPhysChem* **7,** 1032–1035 (2006).
22. Nørskov, J. K. *et al.* Origin of the overpotential for oxygen reduction at a fuel-cell cathode. *J. Phys. Chem. B* **108,** 17886–17892 (2004).
23. Casado-Rivera, E. *et al.* Electrocatalytic activity of ordered intermetallic phases for fuel cell applications. *J. Am. Chem. Soc.* **126,** 4043–4049 (2004).
24. Markovic, N. M. & Ross, P. N. Surface science studies of model fuel cell electrocatalysts. *Surf. Sci. Rep.* **45,** 121–229 (2002).
25. Schmidt, T. J., Stamenkovic, V. R., Lucas, C. A., Markovic, N. M. & Ross, P. N. Surface processes and electrocatalysts on the Pt(hkl)/Bi-solution interface. *Phys. Chem. Chem. Phys.* **3,** 3879–3890 (2001).
26. Gómez, R., Fernández-Vega, A., Feliu, J. M. & Aldaz, A. Hydrogen evolution on Pt single-crystal surfaces—effects of irreversibly adsorbed bismuth and antimony on hydrogen adsorption and evolution on Pt(100). *J. Phys. Chem.* **97,** 4769–4776 (1993).
27. Gómez, R., Feliu, J. M. & Aldaz, A. Effects of irreversibly adsorbed bismuth on hydrogen adsorption and evolution on Pt(111). *Electrochim. Acta* **42,** 1675–1683 (1997).
28. Bowles, B. J. Formation and desorption of monolayers of bismuth on a platinum electrode. *Electrochim. Acta* **15,** 737 (1970).
29. Clavilier, J., Feliu, J. M. & Aldaz, A. An irreversible structure sensitive adsorption step in bismuth underpotential deposition at platinum-electrodes. *J. Electroanal. Chem.* **243,** 419–433 (1988).
30. Hayden, B. E., Murray, A. J., Parsons, R. & Pegg, D. J. UHV and electrochemical transfer studies on Pt(110)-(1x2): The influence of bismuth on hydrogen and oxygen adsorption, and the electro-oxidation of carbon monoxide. *J. Electroanal. Chem.* **409,** 51–63 (1996).
31. Evans, R. W. & Attard, G. A. The redox behavior of compressed bismuth overlayers irreversibly adsorbed on Pt(111). *J. Electroanal. Chem.* **345,** 337–350 (1993).
32. Hamm, U. W., Kramer, D., Zhai, R. S. & Kolb, D. M. On the valence state of bismuth adsorbed on a Pt(111) electrode: an electrochemistry, LEED, and XPS study. *Electrochim. Acta* **43,** 2969–2978 (1998).
33. Kizhakevariam, N. & Stuve, E. M. Coadsorption of bismuth with electrocatalytic molecules—a study of formic-acid oxidation on Pt(100). *J. Vac. Sci. Technol. A* **8,** 2557–2562 (1990).
34. Vetter, K. J. *Electrochemical Kinetics: Theoretical and Experimental Aspects* (Academic, New York, 1967).
35. Paffett, M. T., Campbell, C. T. & Taylor, T. N. The influence of adsorbed Bi on the chemisorption properties of Pt(111)—H_2, CO, and O_2. *J. Vac. Sci. Technol. A* **3,** 812–816 (1985).
36. Paffett, M. T., Campbell, C. T. & Taylor, T. N. Adsorption and growth modes of Bi on Pt(111). *J. Chem. Phys.* **85,** 6176–6185 (1986).
37. Hammer, B., Hansen, L. B. & Nørskov, J. K. Improved adsorption energetics within density-functional theory using revised Perdew-Burke-Ernzerhof functionals. *Phys. Rev. B* **59,** 7413–7421 (1999).
38. Bengtsson, L. Dipole correction for surface supercell calculations. *Phys. Rev. B* **59,** 12301–12304 (1999).
39. Vanderbilt, D. Soft self-consistent pseudopotentials in a generalized eigenvalue formalism. *Phys. Rev. B* **41,** 7892–7895 (1990).
40. Kresse, G. & Furthmuller, J. Efficiency of ab-initio total energy calculations for metals and semiconductors using a plane-wave basis set. *Comput. Mater. Sci.* **6,** 15–50 (1996).
41. Humphrey, W., Dalke, A. & Schulten, K. VMD—visual molecular dynamics. *J. Mol. Graph.* **14,** 33–38 (1996).

Acknowledgements

J.G. and T.F.J. acknowledge H. C. Ørsted Postdoctoral Fellowships from the Technical University of Denmark. J.B. acknowledges support from the Danish Strategic Research Council. The Center for Individual Nanoparticle Functionality is supported by the Danish National Research Foundation. The Center for Atomic-scale Materials Design is supported by the Lundbeck Foundation. We thank the Danish Center for Scientific Computing for computer time. We also thank K. P. Jørgensen and J. Larsen for technical assistance.
Correspondence and requests for materials should be addressed to J.K.N.
Supplementary Information accompanies this paper on www.nature.com/naturematerials.

Competing financial interests

The authors declare that they have no competing financial interests.